

## Free convection boundary-layer flow of a micropolar fluid from a vertical flat plate

D. A. S. REES

*School of Mechanical Engineering, University of Bath,  
Claverton Down, Bath BA2 7AY*

AND

I. POP

*Faculty of Mathematics, University of Cluj, R3400 Cluj, CP253, Romania*

[Received 14 March 1996 and in revised form 7 August 1997]

We examine theoretically the steady free convection from a vertical isothermal flat plate immersed in a micropolar fluid. The governing non-similar boundary-layer equations are derived and are found to involve two material parameters,  $K$  and  $n$ . These equations are solved numerically using the Keller-box method for a range of values of both parameters. A novel feature of the numerical solution is that the boundary layer develops a two-layer structure far from the leading edge. This structure is analysed using asymptotic methods and it is shown that there are two different cases to be considered, namely when  $n \neq \frac{1}{2}$  and when  $n = \frac{1}{2}$ . The agreement between the numerical results and the asymptotic analysis is found to be excellent in both cases. The present paper enables a complete description of the flow to be made for all values of  $K$  and  $n$ , and for all distances from the leading edge for which the boundary-layer approximation is valid.

### 1. Introduction

It is well known that the classical Navier–Stokes theory does not describe adequately the flow properties of polymeric fluids, fluids containing certain additives, and some naturally occurring fluids such as animal blood. Micropolar fluid theory has been used to describe in detail the effect of the presence of dirt in journal bearings (Allen & Kline, 1971; Prakash & Sinha, 1975; Tipei, 1979; Khonsari, 1990). Straughan (1992) also points out that the presence of dust or smoke particles in a gas may also be modelled using micropolar fluid dynamics. The theory of micropolar fluids, first proposed by Eringen (1966), is capable of describing such fluids. In this theory the local effects arising from the microstructure and the intrinsic motion of the fluid elements are taken into account. Physically, the micropolar fluid can consist of a suspension of small, rigid, cylindrical elements such as large dumbbell-shaped molecules. The theory of micropolar fluids is generating a very much increased interest and many classical flows are being re-examined to determine the effects of the fluid microstructure. Early studies along these lines may be found in the review article by Ariman *et al* (1973).

Peddiesen and McNitt (1970) applied the micropolar boundary-layer theory to the problems of steady stagnation point flow, steady flow over a semi-infinite flat plate, and impulsive flow past an infinite flat plate. Gorla (1983) investigated the steady boundary-layer flow of a micropolar fluid at a two-dimensional stagnation point on a moving wall and claimed that the micropolar fluid model is capable of predicting results which exhibit

turbulent flow characteristics, although it is difficult to see how a steady laminar boundary-layer flow could 'appear' to be turbulent.

Thermal boundary-layer flows along a flat plate immersed in a micropolar fluid form a fundamental problem which has attracted significant attention since the early studies of Eringen (1966, 1972). Results for this generic problem have been reported by several investigators, including Jena & Mathur (1981, 1982), Gorla (1988, 1992), Arafa & Gorla (1992) and Chiu & Chou (1993, 1994). However, a very recent work by Rees & Bassom (1996) on the Blasius boundary-layer flow over a flat plate suggests that much more information about the solution of boundary-layer flows of a micropolar fluid can be obtained. In that paper the authors found that a two-layer structure develops as the distance downstream of the leading edge increases, and an asymptotic analysis of the structure was presented. The existence of an inner, near-wall, layer arises because the presence of the wall restricts the rotation of the microelements in the fluid. In the present paper we show that this qualitative behaviour also occurs for the relatively straightforward vertical free convective boundary-layer flow from an isothermal surface. We suspect that it could very well be a general phenomenon.

The objective of this paper, then, is to present numerical results for the problem of natural convection from a vertical, isothermal flat plate immersed in a micropolar fluid, and to undertake a detailed asymptotic analysis which would be valid far downstream of the leading edge. The latter analysis is necessary because the numerical results again reveal that a two-layer structure develops as the distance from the leading edge increases. Further, the inner, near-wall layer becomes increasingly thin compared with the boundary-layer thickness and therefore an asymptotic analysis is essential since it is within this very regime that accurate numerical results are increasingly difficult to obtain.

We shall consider various values of the material parameters  $K$  and  $n$ , which are the ratio of the gyroviscosity and the fluid viscosity, and the ratio of the gyration vector component and the fluid shear at a solid boundary, respectively. Hence this paper is an extension and generalization of previous work on this problem. The methods used for the numerical work and the asymptotic analysis are similar to those employed in (Rees & Bassom, 1996) for the Blasius boundary-layer flow over a flat plate.

The plan of the paper is as follows. In Section 2 the governing equations and boundary conditions are described and the non-similar boundary-layer equations are derived. It is shown that the flow reduces to the classical form when the parameter  $K$  is zero, and therefore the flow and temperature fields are unaffected by the microstructure of the fluid, and the microrotation component is a passive quantity. Numerical solutions of the full boundary-layer equations are presented in Section 3. These use the Keller-box method and results are given for a wide range of values of both  $K$  and  $n$ , where  $n$  varies between 0 and 1. The computations show the development of a two-layer structure as the scaled streamwise distance,  $X$ , increases. In Section 4 asymptotic results are presented for large values of  $X$  and it is shown that the agreement between the numerical and asymptotic results is very good. It is also shown that the strength of the inner, near-wall layer depends on the value of  $n$ : when  $n = \frac{1}{2}$  it has a very much weaker effect on the main boundary-layer flow than when  $n \neq \frac{1}{2}$ . This qualitative result is different from that given in (Rees & Bassom, 1996) where Blasius boundary-layer flow of a micropolar fluid is found to reduce to a self-similar form when  $n = \frac{1}{2}$ .

## 2. Governing equations

Consider a semi-infinite vertical heated plate with a constant wall temperature  $T_w$ , immersed in a micropolar fluid of temperature  $T_\infty$ , where  $T_w > T_\infty$ . The governing equations for steady laminar free convection flow of an incompressible micropolar fluid subject to the Boussinesq approximation may be written in the form

$$\bar{u}_{\bar{x}} + \bar{v}_{\bar{y}} = 0, \quad (1)$$

$$\rho(\bar{u}\bar{u}_{\bar{x}} + \bar{v}\bar{u}_{\bar{y}}) = -\bar{p}_{\bar{x}} + (\mu + \kappa)(\bar{u}_{\bar{x}\bar{x}} + \bar{u}_{\bar{y}\bar{y}}) + \rho g \beta (T - T_\infty) + \kappa \bar{N}_{\bar{y}}, \quad (2)$$

$$\rho(\bar{u}\bar{v}_{\bar{x}} + \bar{v}\bar{v}_{\bar{y}}) = -\bar{p}_{\bar{y}} + (\mu + \kappa)(\bar{v}_{\bar{x}\bar{x}} + \bar{v}_{\bar{y}\bar{y}}) - \kappa \bar{N}_{\bar{x}}, \quad (3)$$

$$\rho j (\bar{u}\bar{N}_{\bar{x}} + \bar{v}\bar{N}_{\bar{y}}) = -2\kappa \bar{N} + \kappa(\bar{v}_{\bar{x}} - \bar{u}_{\bar{y}}) + \text{div}(\gamma \nabla \bar{N}), \quad (4)$$

$$\bar{u}T_{\bar{x}} + \bar{v}T_{\bar{y}} = \alpha(T_{\bar{x}\bar{x}} + T_{\bar{y}\bar{y}}), \quad (5)$$

where  $\bar{x}$  and  $\bar{y}$  are the coordinates parallel with and perpendicular to the flat surface, respectively;  $\bar{u}$  and  $\bar{v}$  are the corresponding fluid velocities;  $T$ ,  $\bar{p}$  and  $\bar{N}$  are the temperature, pressure and the component of the gyration vector normal to the  $(x, y)$ -plane;  $g$  is the acceleration due to gravity;  $\rho$ ,  $\mu$ ,  $\alpha$  and  $\beta$  are the density, viscosity, thermal diffusivity and coefficient of cubical expansion of the fluid; and  $j$ ,  $\kappa$  and  $\gamma$  are the microinertia density, vortex viscosity and spin gradient viscosity. Here, the spin gradient viscosity is assumed to be a constant and given by

$$\gamma = (\mu + \kappa/2)j. \quad (6)$$

This latter relation is invoked to allow the field equations to predict the correct behaviour in the limiting case when microstructure effects become negligible, and the microrotation,  $\bar{N}$ , reduces to the angular velocity; see Ahmadi (1976). The boundary conditions to be applied are

$$\begin{aligned} \bar{y} = 0: \quad \bar{u} = \bar{v} = 0, \quad \bar{N} = -n\bar{u}_{\bar{y}}, \quad T = T_w, \\ \bar{y} \rightarrow \infty: \quad \bar{u} \rightarrow 0, \quad \bar{v} \rightarrow 0, \quad \bar{N} \rightarrow 0, \quad T \rightarrow T_\infty. \end{aligned} \quad (7)$$

Equations (1) to (5) may be rendered dimensionless by writing

$$\begin{aligned} (\bar{u}, \bar{v}) &= (g\beta\Delta T l)^{\frac{1}{2}}(u, v), \quad (\bar{x}, \bar{y}) = l(x, y), \\ \bar{p} &= (g\beta\Delta T l)p, \quad T = T_\infty + \Delta T\theta, \quad \bar{N} = (g\beta\Delta T/l)^{\frac{1}{2}}N, \end{aligned} \quad (8)$$

where  $j = l^2$  defines the lengthscale  $l$ , and  $\Delta T = T_w - T_\infty$ . We obtain the following equations:

$$u_x + v_y = 0, \quad (9)$$

$$uu_x + vv_y = -p_x + \left(\frac{K}{\text{Gr}^{\frac{1}{2}}}\right)N_y + \theta + \left(\frac{1+K}{\text{Gr}^{\frac{1}{2}}}\right)(u_{xx} + v_{yy}), \quad (10)$$

$$uv_x + vv_y = -p_y - \left(\frac{K}{\text{Gr}^{\frac{1}{2}}}\right)N_x + \left(\frac{1+K}{\text{Gr}^{\frac{1}{2}}}\right)(v_{xx} + v_{yy}), \quad (11)$$

$$uN_x + vN_y = -\left(\frac{2K}{\text{Gr}^{\frac{1}{2}}}\right)N + \left(\frac{K}{\text{Gr}^{\frac{1}{2}}}\right)(u_x - u_y) + \left(\frac{1 + \frac{1}{2}K}{\text{Gr}^{\frac{1}{2}}}\right)(N_{xx} + N_{yy}), \quad (12)$$

$$u\theta_x + v\theta_y = \left(\frac{1}{\text{Pr Gr}^{\frac{1}{2}}}\right)(\theta_{xx} + \theta_{yy}), \quad (13)$$

where  $\text{Pr} = \nu/\alpha$  is the Prandtl number,  $\text{Gr} = g\beta\Delta T l^3/\nu^2$  is the Grashof number and  $K = \kappa/\mu$ . Here  $\text{Pr}$  and  $\text{Gr}$  have been defined in the same way as for a standard Newtonian fluid; non-zero values of  $K$  cause coupling between the fluid flow and the gyration vector component  $N$ .

We now invoke the boundary-layer approximation by formally letting the Grashof number become asymptotically large. Hence we set,

$$x = \text{Gr} \hat{x}, \quad y = \hat{y}, \quad u = \text{Gr}^{\frac{1}{2}}\psi_{\hat{y}}, \quad v = -\text{Gr}^{-\frac{1}{2}}\psi_{\hat{x}} \quad \text{and} \quad N = \text{Gr}^{\frac{1}{2}}\hat{N}, \quad (14)$$

where  $\psi$  is the streamfunction defined in such a way that equation (9) is identically satisfied. On substituting (14) into equations (10) to (13) and formally letting  $\text{Gr} \rightarrow \infty$  we obtain the following set of equations at leading order:

$$\psi_{\hat{y}}\psi_{\hat{x}\hat{y}} - \psi_{\hat{x}}\psi_{\hat{y}\hat{y}} = (1 + K)\psi_{\hat{y}\hat{y}\hat{y}} + K\hat{N}_{\hat{y}} + \theta, \quad (15)$$

$$\psi_{\hat{y}}\hat{N}_{\hat{x}} - \psi_{\hat{x}}\hat{N}_{\hat{y}} = -K(2\hat{N} + \psi_{\hat{y}\hat{y}}) + (1 + \frac{1}{2}K)\hat{N}_{\hat{y}\hat{y}}, \quad (16)$$

$$\psi_{\hat{y}}\theta_{\hat{x}} - \psi_{\hat{x}}\theta_{\hat{y}} = \text{Pr}^{-1}\theta_{\hat{y}\hat{y}}. \quad (17)$$

The boundary conditions become,

$$\hat{y} = 0: \quad \psi = \psi_{\hat{y}} = 0, \quad \hat{N} = -n\psi_{\hat{y}\hat{y}}, \quad \theta = 1 \quad (18)$$

$$\hat{y} \rightarrow \infty: \quad \psi_{\hat{y}} \rightarrow 0, \quad \hat{N} \rightarrow 0, \quad \theta \rightarrow 0.$$

The standard similarity form of Pohlhausen (1921) may be used to derive the non-similar boundary-layer equations; therefore we set

$$\psi = \xi^{\frac{3}{4}}f(\xi, \eta), \quad \theta = g(\xi, \eta), \quad \hat{N} = \xi^{\frac{1}{4}}h(\xi, \eta), \quad \xi = \hat{x}, \quad \text{and} \quad \eta = \hat{y}/\hat{x}^{\frac{1}{4}}. \quad (19)$$

and the governing equations for boundary-layer flows become

$$(1 + K)f'''' + \frac{3}{4}ff'' - \frac{1}{2}f'f' + Kh' + g = \xi(f'f'_{\xi} - f_{\xi}f''), \quad (20)$$

$$(1 + \frac{1}{2}K)h'' + \frac{3}{4}fh' - \frac{1}{4}hf' = \xi(f'h_{\xi} - f_{\xi}h') + K\xi^{\frac{1}{2}}(2h + f''), \quad (21)$$

$$\text{Pr}^{-1}g'' + \frac{3}{4}fg' = \xi(f'g_{\xi} - f_{\xi}g'), \quad (22)$$

where dashes represent derivatives with respect to  $\eta$ . The boundary conditions are

$$\eta = 0: \quad f = f' = 0, \quad h + nf'' = 0, \quad g = 1, \quad (23)$$

$$\eta \rightarrow \infty: \quad f' \rightarrow 0, \quad h \rightarrow 0, \quad g \rightarrow 0.$$

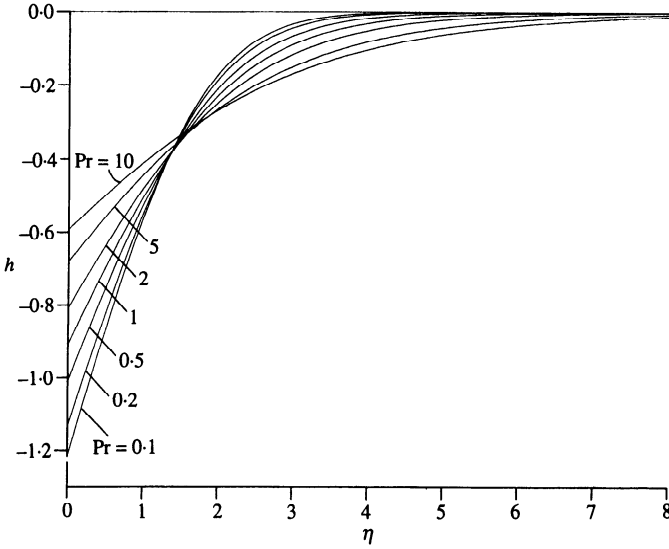


FIG. 1. Profiles of the reduced angular velocity  $h$  as a function of  $\eta$  for different values of  $Pr$  when  $K = 0$  and  $n = 1$

Thus we have a set of parabolic partial differential equations which govern the development of the boundary layer. In general, these equations have to be solved numerically and this, together with an asymptotic analysis for large values of  $\xi$ , will form the substance of this paper.

At this stage it is worthwhile to draw attention to the one case for which equations (20) to (23) are satisfied by a similarity solution. The final term in equation (21) may be regarded as the forcing term in this set of equations, for if it were absent then it is possible that the resulting equations would have a  $\xi$ -independent solution. One possibility is that  $2h + f''$  is identically zero; however, it is easily shown that even when  $n = \frac{1}{2}$  then  $h = -\frac{1}{2}f''$  does not give a consistent set of equations. Therefore we do not obtain a self-similar solution in this way. The second possibility is that  $K = 0$ ; in this case the equation for  $h$  is decoupled from the equations for  $f$  and  $g$ . The resulting similarity solutions satisfy the equations

$$f''' + \frac{3}{4}ff'' - \frac{1}{2}f'f' + g = 0, \tag{24}$$

$$h'' + \frac{3}{4}fh' - \frac{1}{4}hf' = 0, \tag{25}$$

$$Pr^{-1}g'' + \frac{3}{4}fg' = 0 \tag{26}$$

and hence the flow and temperature field are unaffected by the microstructure of the fluid, and the scaled component of the gyration vector  $h$  evolves passively in this case and is given by the solution of (25). The flow and temperature field are given precisely by the solution of Pohlhausen (1921) (but we note that there is a simple numerical scaling difference between Pohlhausen's solution and that given here) and are well known. We have been unable to find a closed-form solution for  $h$ , but a selection of numerical solutions, obtained using a fourth-order Runge-Kutta/shooting method code, are presented in Fig. 1 for  $n = 1$ .

TABLE 1  
*Variation of  $h(0)$ ,  $h'(0)$  and  $g'(0)$  with Pr for  $n = 1$*

Pr	$h(0)$	$h'(0)$	$g'(0)$
0.1	-1.21505	0.71152	-0.16274
0.2	-1.13288	0.63528	-0.21772
0.5	-1.00855	0.52277	-0.31195
0.7	-0.96012	0.48000	-0.35321
1.0	-0.90819	0.43495	-0.40103
2.0	-0.80789	0.35117	-0.50662
5.0	-0.68135	0.25424	-0.67458
6.7	-0.64312	0.22741	-0.73597
10.0	-0.59283	0.19411	-0.82684

Solutions for other values of  $n$  are obtained by multiplying these ' $n = 1$ ' solutions by the required value of  $n$ . The variation of  $h$  with  $\eta$  is shown for various Prandtl numbers. For reference, Table 1 gives the numerical values of  $h(0)$  (which is precisely equal to  $-f''(0)$  when  $n = 1$ ),  $h'(0)$ , and  $g'(0)$ .

### 3. Numerical solution

An examination of equation (21) shows that the final term involves  $\xi^{\frac{1}{2}}$  as a factor. Numerically, this gives rise to large errors near the beginning of the computation since it is difficult to resolve well a function with an infinite slope. Therefore we have deemed it necessary to introduce one further transformation to remove this singularity. On setting

$$X = \xi^{\frac{1}{2}} \quad (27)$$

we obtain

$$(1 + K)f''' + \frac{3}{4}ff'' - \frac{1}{2}f'f' + Kh' + g = \frac{1}{2}X(f'f'_X - f_Xf''), \quad (28)$$

$$(1 + \frac{1}{2}K)h'' + \frac{3}{4}fh' - \frac{1}{4}hf' = \frac{1}{2}X(f'h_X - f_Xh') + KX(2h + f''), \quad (29)$$

$$\text{Pr}^{-1}g'' + \frac{3}{4}fg' = \frac{1}{2}X(f'g_X - f_Xg'). \quad (30)$$

These equations subject to the boundary conditions (23) were solved numerically using the Keller-box method. A non-uniform grid of 78 points was used in the  $\eta$ -direction with the grid points concentrated towards  $\eta = 0$  in order to resolve well the developing near-wall layer mentioned earlier; the maximum value of  $\eta$  used was 100. In the  $X$ -direction a non-uniform grid of 133 points was used with the maximum value of  $X$  being 10000. Newton-Raphson iteration at each streamwise station was used to solve the nonlinear difference equations, and convergence was deemed to have taken place when the maximum absolute pointwise change between successive iterates was  $10^{-10}$ . Double precision arithmetic was used throughout. In all the computations presented here the Prandtl numbers corresponding to water, 6.7, and air, 0.7, were taken.

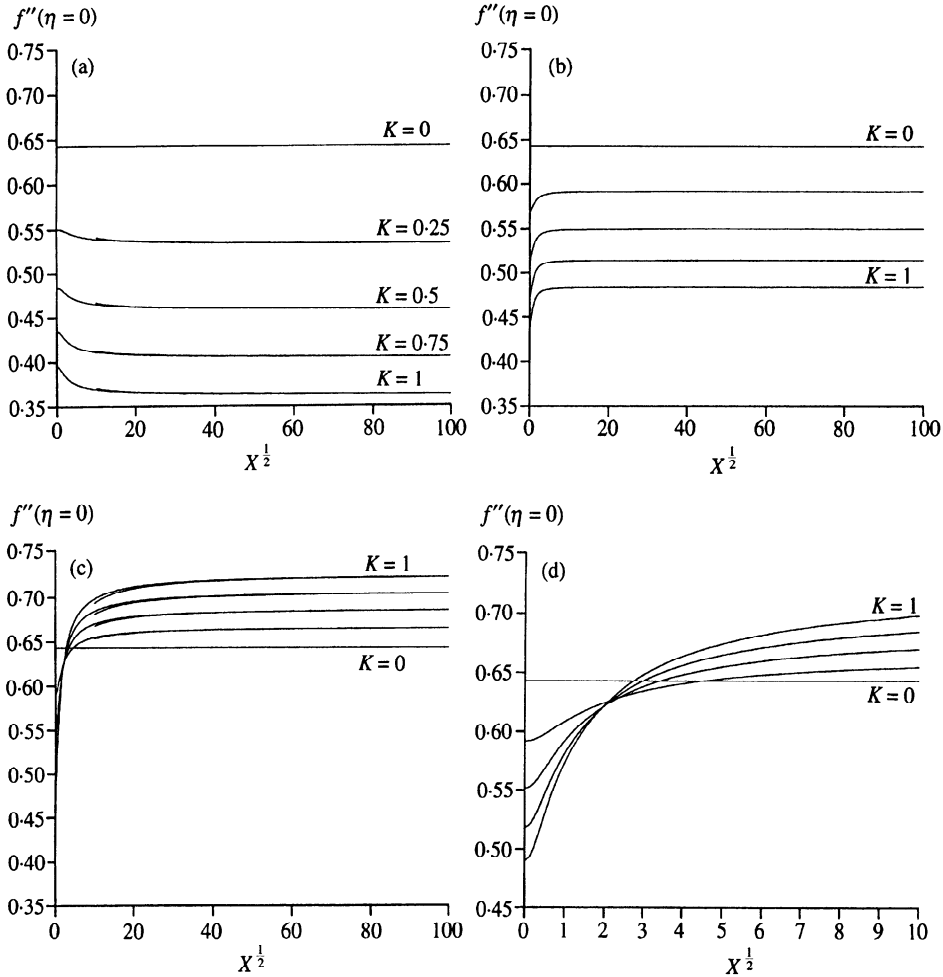


FIG. 2. Evolution with  $X^{1/2}$  of the shear stress,  $f''$  at  $\eta = 0$  for  $Pr = 6.7$ . Also shown are the asymptotic solutions obtained from either (68a) or (84a); these curves lie in the range  $X^{1/2} \geq 10$ . (a)  $n = 0$ ; (b)  $n = \frac{1}{2}$ ; (c)  $n = 1$ ; (d) a close-up view of (c) near  $X = 0$

Our detailed numerical computations are shown in Figs 2 to 5. Figures 2a, 2b and 2c depict the variation of shear stress with  $X$  for  $Pr = 6.7$  and  $K = 0, 0.25, 0.5, 0.75$  and  $1.0$ , for the respective cases  $n = 0, n = 0.5$  and  $n = 1$ . The corresponding rates of heat transfer are given in Figs 3a, 3b and 3c. Note that all these curves are plotted against  $X^{1/2}$  in order to resolve easily the quick variations near  $X = 0$  and the slow approach to the asymptotic solutions developed in the next section.

For all the three values of  $n$  used in Figs 2 and 3 it is readily seen that the curve corresponding to  $K = 0$  is a straight line, a result which is in accord with our earlier observation that  $K = 0$  represents the only self-similar case. When  $K$  is non-zero the form of the shear stress variation depends very much on the values of  $n$  and  $K$ . It is always less than the

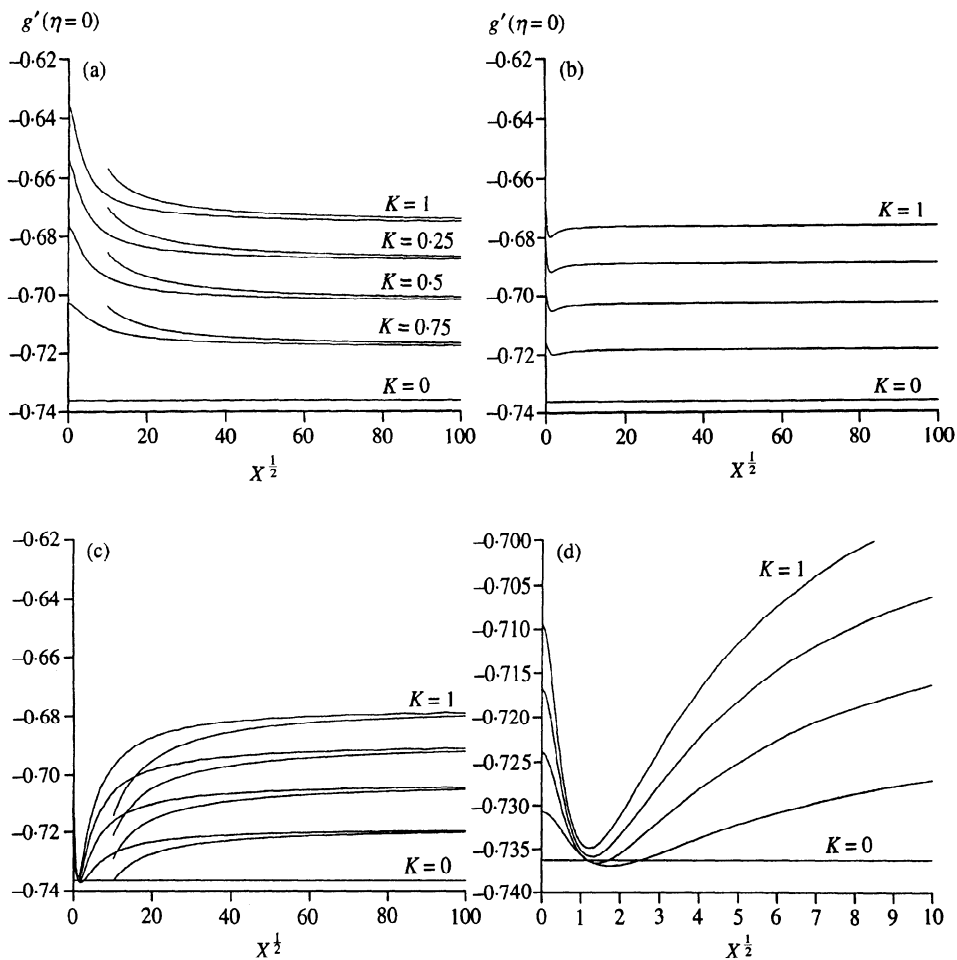


FIG. 3. Evolution with  $X^{\frac{1}{2}}$  of the rate of heat transfer,  $g'$  at  $\eta = 0$  for  $Pr = 6.7$ . Also shown are the asymptotic solutions obtained from either (68b) or (84b); these curves lie in the range  $X^{\frac{1}{2}} \geq 10$ . (a)  $n = 0$ ; (b)  $n = \frac{1}{2}$ ; (c)  $n = 1$ ; (d) a close-up view of (c) near  $X = 0$

$K = 0$  value for sufficiently small  $X$ , but when  $n = 0$  its value decreases further as  $X$  increases, whereas when  $n = 1$  it eventually attains an asymptotic value above the  $K = 0$  result. For low values of  $n$  the spread of the curves for different values of  $K$  is much greater than when  $n = 1$ — Figs 2a, 2b and 2c were plotted using the same ordinate scale in order to emphasize this point.

The detailed evolution of the rate of heat transfer shown in Figs 3a, 3b and 3c are a little more complicated than the shear stress curves. If we refer to the rate of heat transfer in terms of its absolute value, then the  $K \neq 0$  values are always less than the  $K = 0$  value and increase monotonically when  $n = 0$ , implying that the presence of microstructure reduces the rate of heat transfer. When  $n = 1$  the variation is not monotonic; the rate of

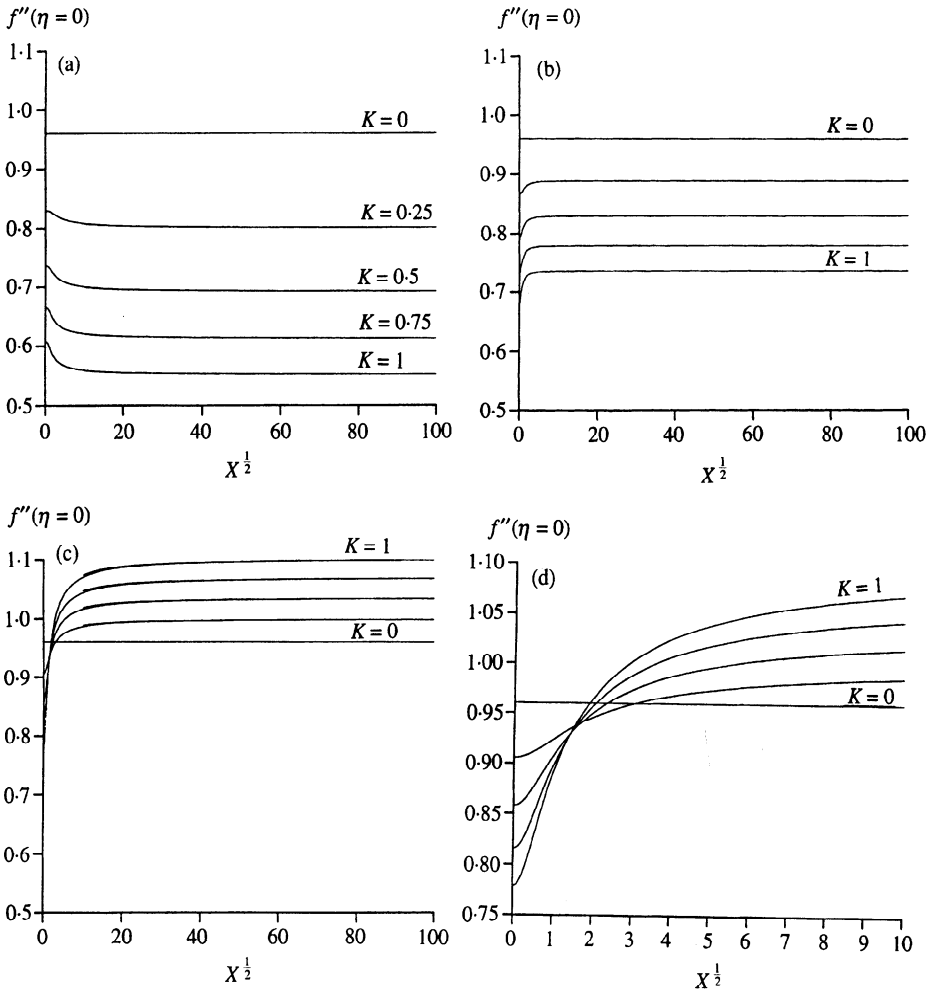


FIG. 4. Evolution with  $X^{1/2}$  of the shear stress,  $f''$  at  $\eta = 0$  for  $Pr = 0.7$ . Also shown are the asymptotic solutions obtained from either (68a) or (84a); these curves lie in the range  $X^{1/2} \geq 10$ . (a)  $n = 0$ ; (b)  $n = \frac{1}{2}$ ; (c)  $n = 1$ ; (d) a close-up view of (c) near  $X = 0$

heat transfer generally remains below the uniform  $K = 0$  rate, but can become slightly greater locally when  $K$  is sufficiently small.

Figures 4 and 5 display the corresponding curves for air where  $Pr = 0.7$ . There is little qualitative difference between the results for water and for air, although the detailed quantitative results are quite different.

In Fig. 6 we display a contour plot of the function  $h + \frac{1}{2}f''$  for the case  $Pr = 0.7$ ,  $K = 1$  and  $n = 1$ . The qualitative nature of this plot is very significant in that it demonstrates the gradual development as  $X$  increases of a thin, near-wall layer embedded within the main boundary layer. Indeed, for the Blasius boundary-layer flow discussed in (Rees & Bassom,

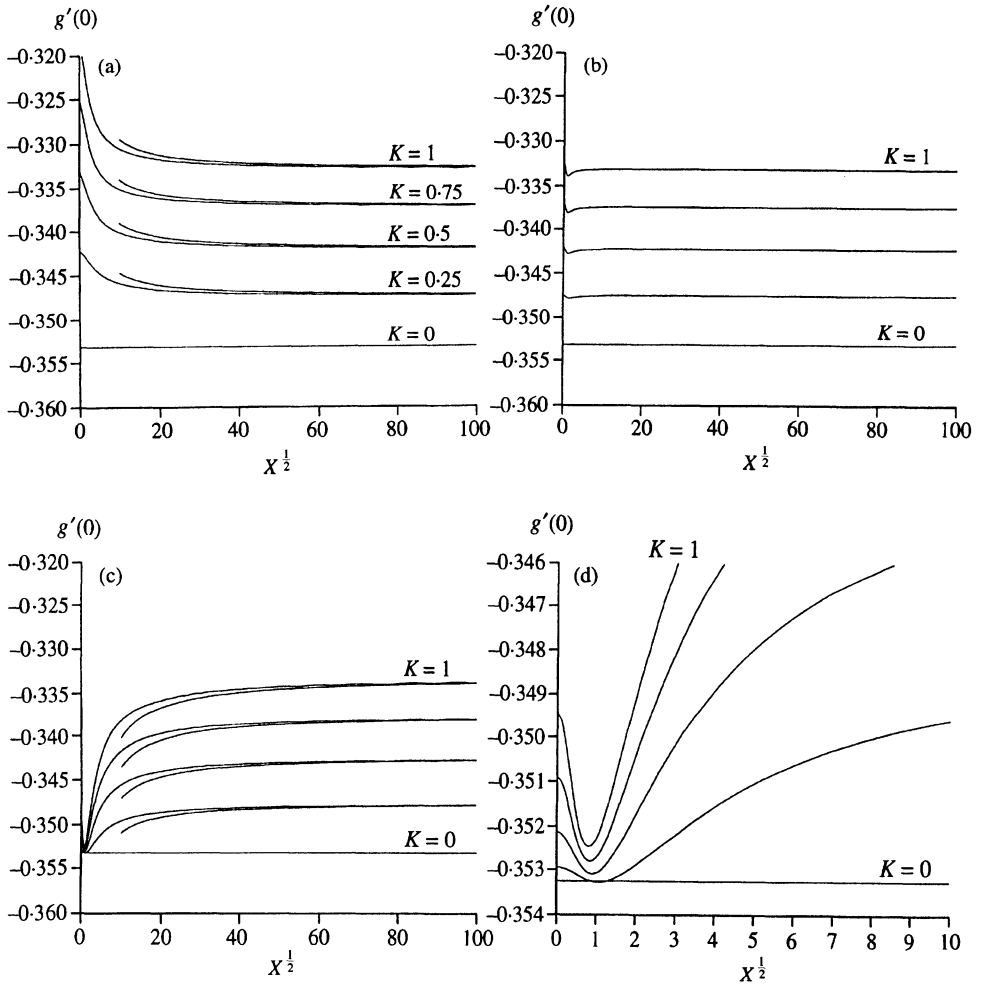


FIG. 5. Evolution with  $X^{\frac{1}{2}}$  of the rate of heat transfer,  $g'(\eta = 0)$  for  $Pr = 0.7$ . Also shown are the asymptotic solutions obtained from either (68b) or (84b); these curves lie in the range  $X^{\frac{1}{2}} \geq 10$ . (a)  $n = 0$ ; (b)  $n = \frac{1}{2}$ ; (c)  $n = 1$ ; (d) a close-up view of (c) near  $X = 0$

1996), it was shown that the function  $h + \frac{1}{2}f''$  is precisely zero when  $n = \frac{1}{2}$ , and that the same function is zero except in a thin layer near the flat plate when  $n \neq \frac{1}{2}$ . For the present problem  $h \neq -\frac{1}{2}f''$  even when  $n = \frac{1}{2}$ , but Fig. 6 shows a similar development of a near-wall layer as  $X$  increases. As shall be seen below, the presence of such a sublayer has its origins in the fact that the boundary condition  $h - nf'' = 0$  at  $\eta = 0$  forces  $h - \frac{1}{2}f''$  to be non-zero near the heated surface. When  $n = \frac{1}{2}$  the same observation applies, but not at leading order. These matters motivate the detailed asymptotic analysis presented in the next section. It is essential to consider the near-wall layer in order to get good agreement between the numerical computations and the asymptotic results.

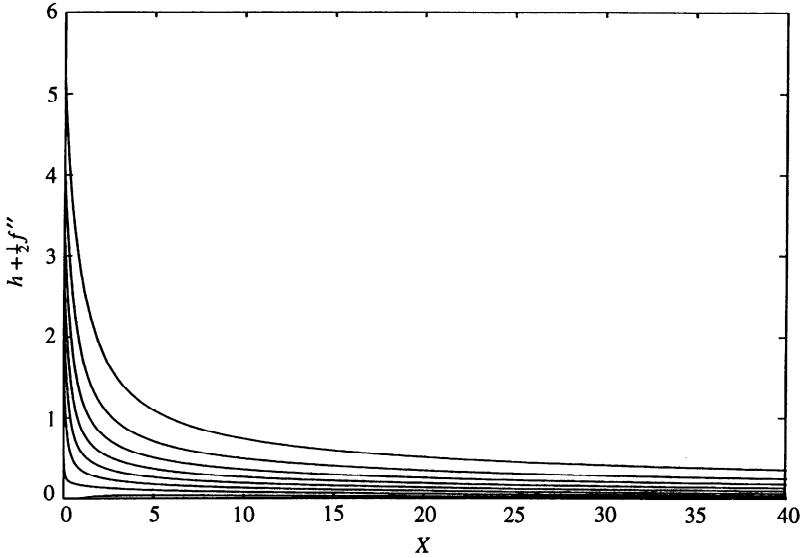


FIG. 6. Contour plot of the function  $h + \frac{1}{2}f''$  for  $Pr = 0.7$ ,  $K = 1$  and  $n = 1$ , showing the development of the near-wall layer as  $X$  increases

**4. Asymptotic solution**

In this section we present an analysis of the boundary layer at asymptotically large distances from the leading edge. In particular we shall determine the thickness of the developing near-wall layer, and compare the theoretical results with the above numerical analysis. In this way we are assured of obtaining a complete description of the flow for all values of  $X$  for which the boundary-layer approximation is valid. We shall use the terms ‘main layer’ and ‘inner layer’ to refer respectively to the main boundary layer where  $\eta = O(1)$  and the near-wall layer where  $\eta$  is asymptotically small.

Given the central role played by the function  $h + \frac{1}{2}f''$  in the analysis of (Rees & Bassom, 1996), we begin by introducing the substitution

$$\phi = h + \frac{1}{2}f'' \tag{31}$$

into equations (28) to (30). The modified equations are

$$(1 + \frac{1}{2}K)f''' + g + K\phi' = \frac{1}{2}f'f' - \frac{3}{4}ff'' + \frac{1}{2}X(f'f'_X - f_Xf''), \tag{32}$$

$$(1 + K)\phi'' + \frac{1}{2}g' - 2KX\phi = \frac{1}{4}\phi f' - \frac{3}{4}f\phi' + \frac{1}{2}X(f'\phi_X - f_X\phi'), \tag{33}$$

$$Pr^{-1}g'' + \frac{3}{4}fg' = \frac{1}{2}X(f'g_X - f_Xg'), \tag{34}$$

and the boundary conditions become,

$$\eta = 0 : \quad f = f' = 0, \quad \phi = (\frac{1}{2} - n)f'', \quad g = 1, \tag{35}$$

$$\eta \rightarrow \infty : \quad f' \rightarrow 0, \quad \phi \rightarrow 0, \quad g \rightarrow 0.$$

For large values of  $X$  it is readily seen that the third term in (33) dominates that equation

unless  $\phi$  is small since  $g' = O(1)$  as  $X \rightarrow \infty$ . Therefore equations (32) to (34) are solved, at least to leading order and for large values of  $X$ , by the expressions,

$$f \sim F_0(\eta) \quad g \sim G_0(\eta) \quad \text{and} \quad \phi \sim \frac{1}{4KX} G'_0(\eta), \quad (36)$$

where  $F_0$  and  $G_0$  are given by

$$(1 + \frac{1}{2}K)F_0''' + \frac{3}{4}F_0F_0'' - \frac{1}{2}F_0'F_0' + G_0 = 0, \quad (37)$$

$$\text{Pr}^{-1}G_0'' + \frac{3}{4}F_0G_0' = 0, \quad (38)$$

subject to

$$\eta = 0 : \quad F_0 = F_0' = 0, \quad G_0 = 1, \quad (39)$$

$$\eta \rightarrow \infty : \quad F_0' \rightarrow 0, \quad G_0 \rightarrow 0.$$

These latter equations are easily written in terms of the classical vertical free convection equations using the transformation

$$F_0(\eta) = (1 + \frac{1}{2}K)^{\frac{1}{2}} \tilde{F}(\tilde{\eta}), \quad G_0(\eta) = \tilde{G}(\tilde{\eta}), \quad \eta = (1 + \frac{1}{2}K)^{\frac{1}{2}} \tilde{\eta}; \quad (40)$$

$\tilde{F}$  and  $\tilde{G}$  satisfy equations which are identical in form to (24) and (26), but where the Prandtl number in (26) is replaced by  $\text{Pr}(1 + \frac{1}{2}K)$ .

An examination of the form of the solution for  $\phi$  in (36) shows that the boundary conditions for  $\phi$  are not satisfied. Even without the numerical evidence presented earlier, it is clear that there must exist a thin layer embedded within the main boundary layer since the highest derivative in equation (33) was neglected when forming the solution for  $\phi$  in (36), and hence this is a singular perturbation problem.

The value of  $n$  now plays an important role in determining the size of  $\phi$  in the inner layer. When  $n = \frac{1}{2}$  we have  $\phi = 0$  at  $\eta = 0$ , and therefore  $\phi = O(X^{-1})$  in this layer in order to match with the form given in (36). But when  $n \neq \frac{1}{2}$  the boundary condition for  $\phi$  states that  $\phi = O(1)$  at  $\eta = 0$ . We therefore have to treat the two cases separately.

Given that the non-satisfaction of the  $\eta = 0$  boundary condition for  $\phi$  is what generates the present singular perturbation problem, it is necessary to determine the asymptotic size of  $\eta$  in the inner layer as  $X \rightarrow \infty$ . On balancing the  $2KX\phi$  and  $\phi''$  terms in (33) we are led to take  $\eta = O(X^{-\frac{1}{2}})$ , and hence the inner-layer variable  $\zeta$  is introduced:

$$\zeta = \eta X^{\frac{1}{2}}. \quad (41)$$

Comparison of the definition of  $\zeta$  with the definitions of  $\eta$  and  $X$  given in (19) and (27) shows that  $\zeta = \hat{y}$ , and therefore the inner layer has a constant thickness. The full boundary-layer equations, (32) to (34), become

$$(1 + \frac{1}{2}K)f''' + X^{-\frac{3}{2}}g + KX^{-1}\phi' = X^{-\frac{1}{2}}(\frac{1}{2}f'f' - \frac{3}{4}ff'') + \frac{1}{2}X^{\frac{1}{2}}(f'f'_X - f_Xf''), \quad (42)$$

$$(1 + K)\phi'' + \frac{1}{2}X^{-\frac{1}{2}}g' - 2K\phi = X^{-\frac{1}{2}}(\frac{1}{4}hf' - \frac{3}{4}fh') + \frac{1}{2}X^{\frac{1}{2}}(f'\phi_X - f_X\phi'), \quad (43)$$

$$\text{Pr}^{-1}g'' + \frac{3}{4}X^{-\frac{1}{2}}fg' = \frac{1}{2}X^{\frac{1}{2}}(f'g_X - f_Xg'), \quad (44)$$

where dashes denote derivatives with respect to  $\zeta$  whenever we are dealing with the inner layer, and with respect to  $\eta$  otherwise. The boundary conditions at  $\zeta = 0$  are

$$f = 0, \quad f' = 0, \quad g = 1 \quad \text{and} \quad \phi = \left(\frac{1}{2} - n\right)f'' \tag{45}$$

Matching conditions obtained from the small- $\eta$  limit of the main-layer solutions will be used to complete the specification of the boundary conditions. The details of the matching conditions will depend on whether or not  $n = \frac{1}{2}$ .

4.1 Case (i):  $n \neq \frac{1}{2}$

For this case we have found that a consistent expansion of the boundary-layer equations in the large  $X$  limit is given by setting

$$f = F_0(\eta) + X^{-\frac{1}{2}}F_1(\eta) + \dots, \tag{46}$$

$$g = G_0(\eta) + X^{-\frac{1}{2}}G_1(\eta) + \dots, \tag{47}$$

$$\phi = X^{-1}\Phi_0(\eta) + X^{-\frac{3}{2}}\Phi_1(\eta) + \dots \tag{48}$$

in the main layer, and

$$f = X^{-1}f_0(\zeta) + X^{-\frac{3}{2}}f_1(\zeta) + \dots, \tag{49}$$

$$g = 1 + X^{-\frac{1}{2}}g_0(\zeta) + X^{-1}g_1(\zeta) + \dots, \tag{50}$$

$$\phi = \phi_0(\zeta) + X^{-\frac{1}{2}}\phi_1(\zeta) + \dots \tag{51}$$

in the inner layer. The equations and boundary conditions for  $F_0$  and  $G_0$  are precisely those given by (37) to (39) whilst  $F_1$  and  $G_1$  satisfy,

$$\left(1 + \frac{1}{2}K\right)F_1''' + G_1 = \frac{3}{4}(F_0'F_1' - F_0F_1'') - \frac{1}{2}F_1F_0'', \tag{52}$$

$$\text{Pr}^{-1}G_1'' + \frac{3}{4}F_0G_1' + \frac{1}{4}F_1G_0' + \frac{1}{4}F_0'G_1 = 0, \tag{53}$$

subject to

$$F_1 = 0, \quad G_1 = 0 \quad \text{at} \quad \eta = 0, \quad \text{and} \quad F_1', G_1 \rightarrow 0 \quad \text{as} \quad \eta \rightarrow \infty. \tag{54}$$

The boundary condition for  $F_1'(0)$ , which is required to complete the solution of (52) and (53), is given by matching with the leading-order inner-layer solution given below.

For large values of  $X$  and for small values of  $\eta$ ,  $f$  and  $g$  may be expanded as follows,

$$\begin{aligned} f &= F_0 + X^{-\frac{1}{2}}F_1 + \dots \\ &= \left[\frac{1}{2}F_0''(0)\eta^2 + \frac{1}{6}F_0'''(0)\eta^3 + \dots\right] + X^{-\frac{1}{2}}\left[\eta F_1'(0) + \frac{1}{2}F_1''(0)\eta^2 + \dots\right] + \dots \\ &= X^{-1}\left[\frac{1}{2}F_0''(0)\zeta^2 + F_1'(0)\zeta + \dots\right] + X^{-\frac{3}{2}}\left[\frac{1}{6}F_0'''(0)\zeta^3 + \frac{1}{2}F_1''(0)\zeta^2 + \dots\right] + \dots, \end{aligned} \tag{55}$$

where the final expression is obtained by rewriting the penultimate expression in terms of the inner-layer variables. Hence (55) gives the required large- $\zeta$  behaviour of the inner-layer solutions.

The inner-layer equations are

$$(1 + \frac{1}{2}K)f_0''' + K\phi_0' = 0, \quad (1 + K)\phi_0'' - 2K\phi_0 = 0, \quad g_0'' = 0, \quad (56)$$

and

$$(1 + \frac{1}{2}K)f_1''' + K\phi_1' = -1, \quad (1 + K)\phi_1'' - 2K\phi_1 = 0, \quad g_1'' = 0, \quad (57)$$

and the boundary conditions at  $\zeta = 0$  are given by

$$f_0 = f_0' = g_0 = f_1 = f_1' = g_1 = 0, \quad \phi_0 = (\frac{1}{2} - n)f_0'' \quad \text{and} \quad \phi_1 = (\frac{1}{2} - n)f_1''. \quad (58)$$

Equations (56) and (57) have the following solutions:

$$f_0 = \frac{1}{2}\zeta^2 F_0''(0) + C F_0''(0)[1 - \lambda\zeta - e^{-\lambda\zeta}], \quad (59)$$

$$g_0 = \zeta G_0'(0), \quad (60)$$

$$\phi_0 = \left(\frac{2 + K}{1 + K}\right) C F_0''(0) e^{-\lambda\zeta}, \quad (61)$$

$$f_1 = -\frac{\zeta^3}{3(2 + K)} + \frac{1}{2}\zeta^2 F_1''(0) + C F_1''(0)[1 - \lambda\zeta - e^{-\lambda\zeta}], \quad (62)$$

$$g_1 = \zeta G_1'(0), \quad (63)$$

$$\phi_1 = \frac{2 + K}{1 + K} C F_1''(0) e^{-\lambda\zeta}, \quad (64)$$

where

$$C = \frac{(\frac{1}{2} - n)(1 + K)}{2[1 + K(1 - n)]} \quad \text{and} \quad \lambda = \left(\frac{2K}{1 + K}\right)^{\frac{1}{2}}. \quad (65)$$

For large values of  $\zeta$  the above solutions for  $f_0$  and  $f_1$ , when substituted into (49), should match with the expression given by (55). Hence we obtain

$$f = X^{-1}[\frac{1}{2}F_0''(0)\zeta^2 - C\lambda F_0''(0)\zeta + \dots] + X^{-\frac{3}{2}}\left[-\frac{1}{3(2+K)}\zeta^3 + \frac{1}{2}F_1''(0)\zeta^2 + \dots\right] + \dots \quad (66)$$

for large values of  $\zeta$ , which, on comparing with (55), yields

$$F_1'(0) = -C\lambda F_0''(0), \quad (67)$$

and therefore we now have all the boundary conditions to be able to solve (52) and (53). In turn, the solutions of (52) and (53) yield the values of  $F_1''(0)$  and  $G_1'(0)$  needed to specify precisely the solutions given in (62) to (64).

It is interesting to note that the solutions for  $g_0$  and  $g_1$  given in (60) and (63) show that the temperature field is passive in the inner layer, at least to second order in the perturbation series.

TABLE 2  
*Variation of  $F''_0(0)$ ,  $G'_0(0)$ ,  $F''_1(0)$  and  $G'_1(0)$  with  $K$  for  $Pr = 6.7$*

$K$	$F''_0(0)$	$G'_0(0)$	$F''_1(0)$	$G'_1(0)$
0.00	0.64312	-0.73597	0.65886	0.97683
0.25	0.59216	-0.71827	0.58101	0.90901
0.50	0.54989	-0.70265	0.51886	0.85253
0.75	0.51418	-0.68868	0.46725	0.80107
1.00	0.48355	-0.67608	0.42582	0.76234

The shear stress and rate of heat transfer may now be computed from the above information. We obtain the formulae

$$\begin{aligned} \frac{\partial^2 f}{\partial \eta^2} \Big|_{\eta=0} &= \left[ \frac{\partial^2 f_0}{\partial \zeta^2} + X^{-\frac{1}{2}} \frac{\partial^2 f_1}{\partial \zeta^2} + \dots \right]_{\zeta=0} \\ &= \frac{(2 + K)}{2[1 + K(1 - n)]} [F''_0(0) + X^{-\frac{1}{2}} F''_1(0) + \dots] \end{aligned} \tag{68a}$$

$$\begin{aligned} \frac{\partial g}{\partial \eta} \Big|_{\eta=0} &= \left[ \frac{\partial g_0}{\partial \zeta} + X^{-\frac{1}{2}} \frac{\partial g_1}{\partial \zeta} + \dots \right]_{\zeta=0} \\ &= G'_0(0) + X^{-\frac{1}{2}} G'_1(0) + \dots \end{aligned} \tag{68b}$$

The form of these expressions suggests that the detailed values of the shear stress and the rate of heat transfer are functions of the three parameters  $K$ ,  $n$  and  $Pr$ . However, it is possible to reduce the problem to one containing only two independent parameters, as follows. The functions,  $F_1$  and  $G_1$ , satisfy linear equations and the boundary condition (67) shows that they must be proportional to  $C\lambda$  since all the remaining boundary conditions are homogeneous. Thus, for any pair of values of  $K$  and  $Pr$ , it is sufficient only to solve for  $F_1$  and  $G_1$  subject to the boundary condition

$$F'_1(0) = -F''_0(0), \tag{69}$$

and then multiply the result by  $C\lambda$ . Tables 2 and 3 give the values of  $F''_1(0)$  and  $G'_1(0)$  obtained in this way, together with the values of  $F''_0(0)$  and  $G'_0(0)$  for both the chosen values of  $Pr$ .

The asymptotic solutions according to equations (68) were computed using the data given in Tables 2 and 3, and are plotted together with the numerically obtained solutions in Figs 2 to 5. In all cases the agreement between the numerical and asymptotic solutions is very good, although it should be noted that if we had presented only a 1-term asymptotic solution, then the agreement would have been very considerably poorer.

TABLE 3  
*Variation of  $F_0''(0)$ ,  $G_0'(0)$ ,  $F_1''(0)$  and  $G_1'(0)$  with  $K$  for  $Pr = 0.7$*

$K$	$F_0''(0)$	$G_0'(0)$	$F_1''(0)$	$G_1'(0)$
0.00	0.96012	-0.35321	0.58312	0.17646
0.25	0.88908	-0.34745	0.52041	0.17419
0.50	0.82973	-0.34223	0.47600	0.15778
0.75	0.77926	-0.33746	0.43505	0.15043
1.00	0.73573	-0.33306	0.40010	0.14436

4.2 Case (ii):  $n = \frac{1}{2}$

When  $n = \frac{1}{2}$  many of the terms in the above analysis become zero, and therefore this case must be considered separately. It may be shown that the appropriate expansions take the form

$$f = F_0(\eta) + X^{-\frac{1}{2}}F_1(\eta) + X^{-1}F_2(\eta) + \dots, \tag{70}$$

$$g = G_0(\eta) + X^{-\frac{1}{2}}G_1(\eta) + X^{-1}G_2(\eta) + \dots, \tag{71}$$

$$\phi = X^{-1}\Phi_0(\eta) + X^{-\frac{3}{2}}\Phi_1(\eta) + X^{-2}\Phi_2(\eta) + \dots \tag{72}$$

in the main layer, and

$$f = X^{-1}f_0(\zeta) + X^{-\frac{3}{2}}f_1(\zeta) + X^{-2}f_2(\zeta) + \dots, \tag{73}$$

$$g = 1 + X^{-\frac{1}{2}}g_0(\zeta) + X^{-1}g_1(\zeta) + X^{-\frac{3}{2}}g_2(\zeta) + \dots, \tag{74}$$

$$\phi = X^{-1}\phi_0(\zeta) + X^{-\frac{3}{2}}\phi_1(\zeta) + X^{-2}\phi_2(\zeta) + \dots \tag{75}$$

in the inner layer. On substituting (70) to (72) into (32) to (34) we find that  $F_0$ ,  $G_0$  and  $\Phi_0$  satisfy equations (37), (38) and (36c) and boundary conditions (39); that  $F_1 = G_1 = \Phi_1 = 0$ ; and that  $F_2$ ,  $G_2$  and  $\Phi_2$  satisfy

$$(1 + \frac{1}{2}K)F_2''' + G_2 + K\Phi_0' = \frac{1}{2}F_0'F_2' - \frac{3}{4}F_0F_2'' - \frac{1}{4}F_2F_0'', \tag{76}$$

$$Pr^{-1}G_2'' + \frac{3}{4}F_0G_2' + \frac{1}{2}F_0'G_2 + \frac{1}{4}F_2G_0' = 0, \tag{77}$$

and

$$\Phi_2 = \frac{1}{2K}(\frac{1}{2}G_2' + (1 + K)\Phi_0'' + \frac{1}{4}F_0'\Phi_0 + \frac{3}{4}F_0\Phi_0'), \tag{78}$$

subject to the boundary conditions,

$$\eta = 0 : F_2 = 0, \quad F_2' = 0, \quad G_2 = 0, \tag{79}$$

$$\eta \rightarrow \infty : F_2' \rightarrow 0, \quad G \rightarrow 0. \tag{80}$$

Note that the boundary condition on  $F_2'$  at  $\eta = 0$  does not arise directly from the application of the no-slip condition, but is derived using the above asymptotic matching techniques from the behaviour of the inner-layer solutions.

TABLE 4  
*Variation of  $F_2''(0) + G_0'(0)/2(2 + K)$  and  $G_2'(0)$  with  $K$  for  $Pr = 6.7$*

$K$	$F_2''(0) + G_0'(0)/2(2 + K)$	$G_2'(0)$
0.25	-0.088844	-0.035136
0.50	-0.076850	-0.033060
0.75	-0.067388	-0.031269
1.00	-0.059763	-0.029704

In the inner layer the solutions are

$$f_0 = \frac{1}{2} F_0''(0) \zeta^2, \quad g_0 = G_0'(0) \zeta, \quad \phi_0 = \frac{G_0'(0)}{4K} (1 - e^{-\lambda \zeta}), \quad (81)$$

$$f_1 = -\frac{\zeta^3}{3(2 + K)}, \quad g_1 = 0, \quad \phi_1 = 0, \quad (82)$$

and

$$f_2 = -\frac{\zeta^4 G_0'(0)}{12(2 + K)} + \frac{1}{2} F_2''(0) \zeta^2 - \left( \frac{1 + K}{2 + K} \right) \frac{G_0'(0)}{4K} (1 - \lambda \zeta - e^{-\lambda \zeta}), \quad (83a)$$

$$g_2 = G_2'(0) \zeta, \quad \phi_2 = \frac{G_2'(0)}{4K} (1 - e^{-\lambda \zeta}). \quad (83b, c)$$

From these solutions it can be seen that the leading-order inner-layer streamfunction and temperature terms,  $f_0$  and  $g_0$ , are passive quantities in the sense that they are precisely the small- $\eta$  versions of the leading-order main-layer solutions. However,  $\phi_0$  has to undergo an adjustment in order to match asymptotically with the main-layer solution and to satisfy the boundary condition at  $\zeta = 0$ . Thus the effect of the inner-layer is considerably weaker when  $n = \frac{1}{2}$  than when  $n \neq \frac{1}{2}$ .

The shear stress and rate of heat transfer are now given by

$$\frac{\partial^2 f}{\partial \eta^2} \Big|_{\eta=0} = F_0''(0) + X^{-1} \left( F_2''(0) + \frac{G_0'(0)}{2(2 + K)} \right) + \dots, \quad (84a)$$

$$\frac{\partial g}{\partial \eta} \Big|_{\eta=0} = G_0'(0) + X^{-1} G_2'(0) + \dots \quad (84b)$$

Tables 4 and 5 present values of  $F_2''(0) + G_0'(0)/2(2 + K)$  and  $G_2'(0)$  needed to obtain the asymptotic shear stress and rate of heat transfer, for both values of the Prandtl number. The appropriate values of  $F_0''(0)$  and  $G_0'(0)$  are given in Tables 2 and 3.

Asymptotic curves for  $n = \frac{1}{2}$  are plotted in Figs 2b, 3b, 4b and 5b, but the agreement with the fully numerical solution is sufficiently close that they are virtually indistinguishable for  $X \geq 100$ .

TABLE 5  
*Variation of  $F_2''(0) + G_0'(0)/2(2 + K)$  and  $G_2'(0)$  with  $K$  for  $Pr = 0.7$*

$K$	$F_2''(0) + G_0'(0)/2(2 + K)$	$G_2'(0)$
0.25	-0.059921	-0.0035284
0.50	-0.052471	-0.0033916
0.75	-0.046501	-0.0032687
1.00	-0.041622	-0.0031576

## 5. Conclusion

In this paper we have sought to analyse in detail the micropolar analogue of the classical vertical free convection boundary-layer flow. The presence of micropolar effects serves to cause the boundary layer (i) to become non-similar, and (ii) to form a well-defined two-layer structure at large distances from the leading edge. An asymptotic analysis showed that the near-wall layer is of constant thickness, and it is the region where the microelements adjust from their natural free-stream orientation to that imposed by the presence of the solid boundary. Numerical results obtained using the Keller-box method were, in all cases, found to give very good comparisons with the asymptotic analysis. It was found that the detailed results depend very much on the values of  $K$  and  $Pr$ , and especially on whether or not  $n$  is equal to  $\frac{1}{2}$ . When  $n = \frac{1}{2}$  the inner layer is considerably weaker than when  $n \neq \frac{1}{2}$ .

Finally it is of interest to query why the two-layer asymptotic structure was not found in the mixed convection analysis of Gorla, Lin & Yang (1990). In that paper the authors showed correctly that forced convection effects dominate near the leading edge, but that free convection dominates further downstream. In fact they show that the asymptotic profile is self-similar. This latter conclusion is seemingly at variance with the results of the present paper, but they may be reconciled by noting that the analysis of (Gorla *et al.*, 1990), when translated into the present notation, is equivalent to having  $x = O(1)$ , see equation (14). Thus, their analysis is entirely correct as far as it goes, which is to consider large values of  $x$  within the  $O(1)$  regime. We have therefore extended their work by looking at  $x = O(Gr)$  distances where microinertia effects serve to stratify the boundary layer.

## REFERENCES

- AHMADI, G. 1976 Self-similar solution of incompressible micropolar boundary layer flow over a semi-infinite flat plate. *Int. J. Engng Sci.* **14**, 639–646.
- ALLEN, S. & KLINE, K. 1971 Lubrication theory for micropolar fluids. *Trans. A.S.M.E. J. Appl. Mech.* **38**, 646–650.
- ARAF, A. A. & GORLA, R. S. R. 1992 Mixed convection boundary layer flow of a micropolar fluid along vertical cylinders and needles. *Int. J. Engng Sci.* **30**, 1745–1751.
- ARIMAN, T., TURK, M. A. & SYLVESTER, N. D. 1973 Microcontinuum fluid mechanics—a review. *Int. J. Engng Sci.* **11**, 905–930.
- CHIU, C.-P. & CHOU, H.-M. 1993 Free convection in the boundary layer flow of a micropolar fluid along a vertical wavy surface. *Acta Mech.* **101**, 161–174.

- CHIU, C.-P. & CHOU, H.-M. 1994 Transient analysis of natural convection along a vertical wavy surface in micropolar fluids *Int. J. Engng Sci.* **32**, 19–33.
- ERINGEN, A. C. 1966 Theory of micropolar fluids. *J. Math. Mech.* **16**, 1–18.
- ERINGEN, A. C. 1972 Theory of thermomicropolar fluids. *J. Math. Appl. Anal.* **38**, 480–496.
- GORLA, R. S. R. 1983 Micropolar boundary layer at a stagnation point. *Int. J. Engng Sci.* **21**, 25–34.
- GORLA, R. S. R. 1988 Combined forced and free convection in micropolar boundary layer flow on a vertical flat plate. *Int. J. Engng Sci.* **26** 385–391.
- GORLA, R. S. R. 1992 Mixed convection in a micropolar fluid from a vertical surface with uniform heat flux. *Int. J. Engng Sci.* **30**, 349–358.
- GORLA, R. S. R., LIN, P. P. & YANG, A.-J. 1990 Asymptotic boundary layer solutions for mixed convection from a vertical surface in a micropolar fluid. *Int. J. Engng Sci.* **28**, 525–533.
- JENA, S. K. & MATHUR, M. N. 1981 Similarity solutions for laminar free convection flow of a thermomicropolar fluid past a nonisothermal flat plate. *Int. J. Engng Sci.* **19**, 1431–1439.
- JENA, S. K. & MATHUR, M. N. 1982 Free convection in the laminar boundary layer flow of thermomicropolar fluid past a flat plate with suction/injection. *Acta Mech.* **42**, 227–238.
- KHONSARI, M. M. 1990 On the self-excited whirl orbits of a journal in a sleeve bearing lubricated with micropolar fluids. *Acta Mech.* **81**, 235–244.
- PEDDIESEN, J. & MCNITT, R. P. 1970 Boundary layer theory for a micropolar fluid. *Recent Adv. Eng. Sci.* **5**, 405–476.
- POHLHAUSEN, E. 1921 Der Wärmeaustausch zwischen festen Körpern und Flüssigkeiten mit kleiner Reibung und kleiner Wärmeleitung. *Z. Angew. Math. Mech.* **1**, 115–124.
- PRAKASH, J. & SINHA, P. 1975 Lubrication theory for micropolar fluids and its application to a journal bearing. *Int. J. Engng Sci.* **13**, 217–232.
- REES, D. A. S. & BASSOM, A. P. 1996 The Blasius boundary layer flow of a micropolar fluid. *Int. J. Engng Sci.* **34**, 113–124.
- STRAUGHAN, B. 1992 *The Energy Method, Stability, and Nonlinear Convection*. Applied Mathematical Sciences 91. Berlin: Springer.
- TIPEI, N. 1979 Lubrication with micropolar liquids and its application to short bearings *Trans. A.S.M.E. J. Lub. Tech.* **101**, 356–363.